THE JOURNAL OF BIOLOGICAL CHEMISTRY
Vol. 279, No. 13, Issue of March 26, pp. 13044–13053, 2004

Printed in U.S.A.

Investigating Mitochondrial Redox Potential with Redox-sensitive Green Fluorescent Protein Indicators*

Received for publication, November 24, 2003, and in revised form, January 1, 2004
Published, JBC Papers in Press, January 13, 2004, DOI 10.1074/jbc.M312846200

George T. Hanson‡ ‡‡, Robert Aggeler§, Devin Oglesbee§, Mark Cannon‡, Roderick A. Capaldi§, Roger Y. Tsien¶, and S. James Remington‖**

From the §Departments of Biology, ‡Chemistry and ‖Physics, Institute of Molecular Biology, University of Oregon, Eugene, Oregon 97403-1229, and the ¶Department of Chemistry and Biochemistry and Department of Pharmacology, University of California San Diego, La Jolla, California 92093-0647

Current methods for determining ambient redox potential in cells are labor-intensive and generally require destruction of tissue. This precludes single cell or real time studies of changes in redox poise that result from metabolic processes or environmental influences. By substitution of surface-exposed residues on the *Aequorea victoria* green fluorescent protein (GFP) with cysteines in appropriate positions to form disulfide bonds, reduction-oxidation-sensitive GFPs (roGFPs) have been created. roGFPs have two fluorescence excitation maxima at about 400 and 490 nm and display rapid and reversible ratiometric changes in fluorescence in response to changes in ambient redox potential *in vitro* and *in vivo*. Crystal structure analyses of reduced and oxidized crystals of roGFP2 at 2.0- and 1.9-Å resolution, respectively, reveal in the oxidized state a highly strained disulfide and localized main chain structural changes that presumably account for the state-dependent spectral changes. roGFP1 has been targeted to the mitochondria in HeLa cells. Fluorometric measurements on these cells using a fluorescence microscope or in cell suspension using a fluorometer reveal that the roGFP1 probe is in dynamic equilibrium with the mitochondrial redox status and responds to membrane-permeable reductants and oxidants. The roGFP1 probe reports that the matrix space in HeLa cell mitochondria is highly reducing, with a midpoint potential near −360 mV (assuming mitochondrial pH ~8.0 at 37 °C). In other work (C. T. Dooley, T. M. Dore, G. Hanson, W. C. Jackson, S. J. Remington, and R. Y. Tsien, submitted for publication), it is shown that the cytosol of HeLa cells is also unusually reducing but somewhat less so than the mitochondrial matrix.

Most metabolic reactions in cells take place in reducing compartments such as the mitochondria or cytoplasm. This is presumably because critical thiol groups and other key catalytic elements of enzyme active sites must be protected against oxidation. Protein disulfide bonds are rarely found in such environments. On the other hand, normal cell function requires that some compartments, such as the endoplasmic reticulum in eukaryotes, be oxidizing. This is essential for the proper folding and function of proteins destined for export, which frequently contain disulfide bridges.

Much has recently been learned regarding the mechanisms responsible for homeostasis of redox status in certain subcellular compartments. In yeast, the formation of disulfide bonds in the endoplasmic reticulum utilizes conserved Ero1p (2, 3) and/or Erv2p (4, 5), which are FAD-containing enzymes that directly consume molecular oxygen to create a disulfide linkage. In addition, the disulfide exchange component protein-disulfide isomerase ensures formation of the correct disulfides (6) (for reviews, see Refs. 7 and 8). In prokaryotes, a thioredoxin-like family of enzymes catalyzes the formation and isomerization of disulfide bonds in proteins via highly specific disulfide exchange reactions (9).

In all cells, small molecules capable of thiol-disulfide exchange like GSH are abundant and were previously thought to act as redox buffers, but this hypothesis has been disproved. For example, in the protein export pathway, GSH actually competes with protein thiols for oxidizing equivalents (8, 10). Thus, the primary role of small thiols may be one of defense against oxidants and other deleterious compounds (for reviews, see Refs. 2, 11, and 12).

Where required, the general mechanisms responsible for redox homeostasis may also be co-opted for other diverse processes such as apoptosis, disease, oxidative defense mechanisms, allosteric control of enzyme activity, and a variety of signal transduction pathways. For example, oxidative events have been implicated in activating the mitochondrial permeability transition, leading to cytochrome *c* release and cell death (13–15). Changes of the cellular oxidation potential have been suggested to be a final step in the apoptotic process leading to degradation of apoptotic bodies (16). Soluble, short lived, and reactive species such as peroxides (17, 18) and NO (19) are now recognized to be second messengers that can directly modulate the activity of target proteins as well as indirectly couple cellular responses to external events. These processes can result in the nitrosylation or oxidation of specific cysteine residues on a target protein to one of several possible states, directly modulating the activity of target. Signal transduction mechanisms involving such oxidative modifications are now recognized to rival protein phosphorylation in significance.

Given the importance of and general interest in cellular redox processes, a noninvasive method for reporting redox changes within living cells is highly desirable. Until now, no

* This work was supported in part by National Institutes of Health Grants GM-42618 (to S. J. R.), HL-24526 (to R. A. C.), and T32-GM07759 (to G. T. H.). The costs of publication of this article were defrayed in part by the payment of page charges. This article must therefore be hereby marked "*advertisement*" in accordance with 18 U.S.C. Section 1734 solely to indicate this fact.

The atomic coordinates and structure factors (codes 1JC0 and 1JC1) have been deposited in the Protein Data Bank, Research Collaboratory for Structural Bioinformatics, Rutgers University, New Brunswick, NJ (http://www.rcsb.org/). The models summarized in Table II were the result of additional refinement and minor improvements that took place after 1JC0 and 1JC1 were deposited, and the data sets will be updated.

** To whom correspondence should be addressed. Tel.: 541-346-5190; Fax: 541-346-5870; E-mail: jim@uoxray.uoregon.edu.

‡‡ Present address: Invitrogen, 501 Charmany Dr., Madison, WI 53719-1236.

general approach for nondestructive readout of redox status has been available. Whereas several methods of determining *in vivo* redox status have been proposed, all have serious limitations. Most techniques require cells to be harvested before their contents can be analyzed. For example, several attempts have been made to directly measure the ratio of reduced to oxidized glutathione, which is with few exceptions the most abundant nonprotein thiol in eukaryotic cells (20). This ratio has been found to range from 1:1 to 3:1 in the secretory pathway, and in total cellular material it has been found to range from 100:1 to 300:1. Whereas these results point to dramatic differences in redox poise within compartments, with such an approach it is of course impossible to monitor redox changes within the same cell over a period of time. Keese *et al.* (21) proposed an alternative procedure in which crystals of the enzyme glutathione reductase are microinjected into the cytosol of human fibroblasts. By detection of color changes in the crystals, they were able to determine the redox potential of the cytosol to be more reducing than −0.270 V. Whereas this method may allow redox status determination within single living cells, it is cumbersome.

Indicators that give visual response to changes in dynamic redox status can be constructed from the green fluorescent protein (GFP),[1] which has become a popular tool for molecular labeling *in vivo* (for reviews, see Refs. 22–24). GFP is most often used as a passive indicator of gene expression and protein localization, but variants have been constructed that act as indicators of intracellular concentrations of H^+, Ca^{2+}, and halide ions (25–32). The key properties of GFP are efficient fluorescence, protease resistance, and stability throughout a wide range of pH and solvent conditions. Moreover, GFP can be targeted to specific organelles within the host cell, permitting conditions at localized areas to be monitored in a single cell over a period of time.

An indicator for redox status can be constructed from GFP by introduction of redox-reactive groups into the protein, at locations where a change in the oxidation state of the introduced group(s) would modify the fluorescent properties. Ostergaard *et al.* (33) introduced pairs of cysteines onto the surface of yellow fluorescent protein (YFP) (34) in appropriate locations to form disulfide bridges in an oxidizing environment. The indicators, designated rxYFP$^{N}_{M}$ (where *N* and *M* indicate the locations of introduced cysteines) were successfully expressed in the cytoplasm of *Escherichia coli* and were shown to respond, by changes in fluorescence intensity, to membrane-permeable redox agents 4,4′-dithiodipyridine and dithiothreitol (DTT). The indicators also responded to mutational disruption of the *trxB* gene, which codes for the flavoenzyme thioredoxin reductase and is partially responsible for the reducing state of the cytoplasm. Although the results of these efforts are promising, rxYFP$^{N}_{M}$ redox probes suffer from several limitations. Because only the intensity of fluorescence is affected by disulfide bond formation, the probes are not ratiometric and would be difficult to calibrate (32, 35). A further complication arises from the fact that YFP fluorescence is quenched by a low concentration of halides and other small anions (36, 37).

Here, we describe the independent development and preliminary application of several GFP-based indicators of redox status. The indicators are ratiometric by excitation, which reduces or eliminates measurement errors resulting from changes of indicator concentration, photobleaching, and variable cell thickness. Directed substitution of cysteine residues at selected surface sites in the vicinity of the GFP chromophore but upon different GFP backgrounds resulted in indicators with apparent midpoint potentials in the range −0.27 to −0.29 V. We term these probes redox-sensitive GFPs (roGFPs).

Analysis of the oxidized and reduced crystal structures of roGFP2 verified reversible formation of an intramolecular disulfide bridge and revealed an oxidation-dependent strain in the polypeptide backbone that may account for the observed spectral changes. Using cultured mammalian cells expressing roGFP1 in the mitochondria, we show that the probe reversibly reports redox changes in response to application of membrane-permeable oxidizing and reducing agents. Measurements were conducted on single cells using a fluorescence microscope and with cell suspensions in an ordinary fluorometer with comparable results. After correcting for the estimated pH (~8.0) of the mitochondria, the *in vivo* results suggest that the redox potential of resting mitochondria in HeLa cells is near −360 mV.

MATERIALS AND METHODS

Structure-based Design of Redox-sensitive GFP Variants—roGFP indicators were designed with the concept that cross-links between pairs of surface-exposed cysteine residues may induce structural strain in the protein. For locations close to the chromophore, modifications of the chromophore environment can be expected to result in changes in the fluorescence excitation or emission properties. To prevent undesirable cross-link formation, we attempted to replace the two cysteines present in wild-type GFP at positions 48 and 70 (38) by serine and alanine, respectively. The substitution of Cys^{70} proved to be deleterious to obtaining soluble, fluorescent protein, so the C48S construct was used as the background in most cases. Candidate sites for introduction of potential disulfide pairs were selected by visual inspection of the atomic model for S65T GFP (34) (Protein Data Bank code 1EMA) for surface locations with approximately the required separation and orientation for formation of a disulfide linkage (39, 40). The two sets of sites reported in this work included Ser^{147} and Gln^{204} (roGFP1 and -2; see Table I) and Asn^{149} and Ser^{202} (roGFP3 and -4), each flanking His^{148}. The single-cysteine variants were created on either pseudo-wild type background (C48S/Q80R) or (C48S/Q80R/S65T), and their properties were investigated before construction of the double cysteine substitutions. Finally, the double disulfide variant was constructed (roGFP5 and -6) with and without the S65T mutation.

Gene Construction and Protein Expression—Mutations were introduced via the QuikChange™ kit (Stratagene, La Jolla, CA), following the manufacturer's protocol. DNA sequencing of the entire GFP coding sequence verified all mutations. Mutations were initially introduced into a His-tagged version of wild-type (Q80R) GFP in the plasmid pRSET$_B$. For expression in mammalian cells, the mutations C48S/T65S/S147C/Q204C (which contains S65T) and C48S/S147C/Q204C (roGFP1 and -2) were introduced into the plasmid pEGFP-N1 (Clontech) containing in addition the leader sequence of the $E_1\alpha$ subunit of pyruvate dehydrogenase for mitochondrial targeting (a gift of R. M. Brown and G. K. Brown, University of Oxford). The resulting plasmid also contained the so-called "folding mutation" F64L, which seems to improve the efficiency of proper folding and chromophore formation *in vivo* (41). To verify that F64L did not significantly alter the properties of roGFPs, the mutation was introduced into the original pRSET$_B$ plasmid. In side-by-side experiments, roGFP2 and roGFP2/F64L had indistinguishable spectral and redox properties (data not shown).

Mutant protein was expressed in *E. coli* strain JM109(DE3) by use of the pRSET$_B$ expression system with an N-terminal His_6 tag. The cells were resuspended in 50 mM HEPES (pH 7.9), 300 mM NaCl, 10% glycerol, and sonicated for 7 min. Cell lysate was centrifuged, and the supernatant was applied to a column of Ni^{2+}-nitrilotriacetic acid-agarose resin (Qiagen, Hilden, Germany). The N-terminal histidine tag was removed by incubation with 1:50 (w/w) γ-chymotrypsin for 20 h at 22 °C. Samples were concentrated by filtration (Centricon 10; Amicon) and buffer-exchanged with PD-10 Sephadex columns (Amersham Biosciences) into 20 mM HEPES, pH 7.9.

Spectroscopy and Redox Titrations—Fluorescence excitation spectra were collected on Hitachi F4500 and PerkinElmer Life Sciences LS55 fluorescence spectrophotometers at 30 °C. Samples consisted of 1 μM GFP in 75 mM HEPES (pH 7.0), 140 mM NaCl, 1 mM EDTA, and 1 mM total DTT (mixture of oxidized and reduced forms). To reduce air oxidation, the solutions were degassed and subsequently flushed with nitrogen. Where possible, most solutions were prepared and allowed to

[1] The abbreviations used are: GFP, green fluorescent protein; roGFP, redox-sensitive GFP; DTT, dithiothreitol; YFP, yellow fluorescent protein.

equilibrate in a glove box under a nitrogen atmosphere.

In general, equilibrium was obtained within 1 h at pH 7.0. However, the samples were incubated at 30 °C for 4 h to ensure equilibration of the GFP-DTT system. Because the equilibrium constant for the reaction $roGFP_{red} + DTT_{ox} \leftrightarrow roGFP_{ox} + DTT_{red}$ is much less than 1 (see "Results"), the results were checked by performing an alternative titration against reduced and oxidized lipoic acid (10 mM in the above buffer) for roGFP1, as described elsewhere.[2]

The equilibrated reaction mixtures were subjected to SDS-PAGE analysis, which showed no evidence for species corresponding to disulfide-linked dimers (data not shown). Therefore, any disulfides that are formed are intramolecular (see below for crystallographic evidence).

Determination of Midpoint Potentials—Apparent redox midpoint potential values for roGFPs were found by exploiting the fact that the fluorescence excitation spectrum of roGFPs is strongly and reversibly dependent upon the redox state of the introduced cysteines. When equilibrated against redox buffers consisting of reduced and oxidized dithiothreitol (DTT_{red}, DTT_{ox}) or lipoic acid, fluorescence spectra of roGFPs revealed amplitude changes in the two excitation maxima with a well defined isosbestic point. The redox reaction of the roGFPs with reduced and oxidized DTT could thus be analyzed using a two-state model. The equilibrium for the oxidation of reduced roGFP by DTT_{ox} and the corresponding equilibrium constant (K_{eq}) are given by Reaction 1 and Equation 1.

$$roGFP_{red} + DTT_{ox} \leftrightarrow roGFP_{ox} + DTT_{red}$$

REACTION 1

$$K_{eq} = [roGFP_{ox}][DTT_{red}]/[roGFP_{red}][DTT_{ox}] \quad \text{(Eq. 1)}$$

When roGFPs were incubated in the presence of varying concentrations of DTT_{red} and DTT_{ox} (total $DTT_{red} + DTT_{ox} = 1$ mM), the fractional amount of reduced roGFP at equilibrium (R) could be measured over the whole range from the oxidized to the reduced protein using the chromophore fluorescence. Since SDS-PAGE and crystallography revealed that roGFPs form only intramolecular disulfide bonds, R can be related to K_{eq} by Equation 2 (42).

$$R = ([DTT_{red}]/[DTT_{ox}])/(K_{eq} + [DTT_{red}]/[DTT_{ox}]) \quad \text{(Eq. 2)}$$

For experimental determination of the equilibrium constants of the roGFP-dithiothreitol system, the equilibrium concentrations of DTT_{red} and DTT_{ox} were calculated according to Equations 3–5. In these expressions, $[DTT_{red\,o}]$ and $[DTT_{ox\,o}]$ are the initial concentrations of DTT_{red} and DTT_{ox}, respectively, R is the fractional amount of reduced roGFP at equilibrium, $[roGFP_o]$ is the initial concentration of oxidized roGFP, F is a fluorescence intensity ratio of excitation at 490 nm *versus* the isosbestic point (425 nm), and F_{ox} and F_{red} are the 490/425 nm ratios of the completely oxidized and reduced protein, respectively, although any two wavelengths can be chosen.

$$[DTT_{red}] = [DTT_{red\,o}] - R[roGFP_o] \quad \text{(Eq. 3)}$$

$$[DTT_{ox}] = [DTT_{ox\,o}] + R[roGFP_o] \quad \text{(Eq. 4)}$$

$$R = (F - F_{ox})/(F_{red} - F_{ox}) \quad \text{(Eq. 5)}$$

By plotting R against the $[DTT_{red}]/[DTT_{ox}]$ ratio and fitting the data to a titration curve according to Equation 2, the K_{eq} for the roGFP/dithiothreitol system could be found. The redox potential of roGFPs at pH 7 and 30 °C ($E'_{0(roGFP)}$) could then be calculated from the Nernst equation (6), where E'_0 is the biochemist's standard potential of the DTT_{red}/DTT_{ox} couple ($E'_{0(DTT)} = -0.323$ V, at pH 7 and 30 °C (43)), R is the gas constant (8.315 J K^{-1} mol^{-1}), T is the absolute temperature (303.15 K), n is the number of transferred electrons (2), and F is the Faraday constant (9.649×10^4 C mol^{-1}).

$$E'_{0(roGFP)} = E'_{0(DTT)} - (RT/nF) \times \ln K_{eq} \quad \text{(Eq. 6)}$$

Plots and curve fits were made with KaleidaGraph (Abelbeck Software). For the case of titration against reduced/oxidized lipoate, $E'_{0(Lip)} = -0.290$ V (44) was assumed.

Redox potentials involving the liberation of H^+ depend intrinsically on pH. The pH dependence of the midpoint potential can be seen from the half-reaction of roGFP reduction as follows.

$$roGFP_{ox} + 2H^+ + 2e^- \leftrightarrow roGFP_{red}$$

REACTION 2

In equilibrium at the midpoint, $[roGFP_{ox}] = [roGFP_{red}]$ and $K_{eq} = [H^+]^2$. Theoretically, the redox potential of roGFP at 30 °C can thus be calculated from the Nernst equation and E'_0 at any pH using Equation 7.

$$E'^{pH}_0 = E'_0 - 60.1 \text{ mV} \times (\text{pH} - 7) \quad \text{(Eq. 7)}$$

Ratiometric Measurements—The roGFP probes display two fluorescence excitation maxima whose relative amplitudes depend on the specific mutations but also depend on the state of oxidation. This can be used to make ratiometric measurements (35, 45), which reduce or eliminate dependence on protein concentration, sample path length, photobleaching, and variable source intensity. The *in vitro* ratios of the excitation maxima were determined in the fluorometer directly from the excitation spectrum at typically 400 and 475 nm (2.5-nm slit width) for roGFP1 or 400 and 490 nm for roGFP2. The dynamic range parameter δ is defined as the ratio of the maximum to minimum values of the excitation ratios, and is useful as a measure of the maximum attainable signal/noise ratio.

Crystal Structure Determination—roGFP2/F64L (C48S/F64L/S65T/Q80R/S147C/Q204C) was concentrated to ~20 mg ml^{-1} in 20 mM HEPES (pH 7.9) and 0.2-μm-filtered. Flat plate-like crystals grew at room temperature in 1–2 days by hanging drop vapor diffusion against 0.1 M Tris (pH 8.5), 0.07–0.1 M $LiSO_4$, 17–22% polyethylene glycol 4000, and 0.5 μM $CuCl_2$ (which catalyzes disulfide formation) or 5 mM DTT for the oxidized and reduced crystals, respectively. Drops contained 4 μl of protein solution and 4 μl of well solution. For low temperature diffraction data collection, crystals were exchanged into a solution of 0.1 M Tris (pH 8.5), 0.07–0.1 M $LiSO_4$, 20% polyethylene glycol 4000, 20% ethylene glycol, and either 0.5 μM $CuCl_2$ or 5 mM DTT.

X-ray diffraction data were collected from a single frozen crystal for each redox state at beamline 7-1 at the Stanford Synchrotron Radiation Laboratory. Data sets were indexed and reduced with MOSFLM (46), and intensities were scaled with SCALA (CCP4 program suite). Molecular replacement solutions were found with EPMR (47), using the GFP S65T coordinate file (Protein Data Bank code 1EMA) as the search model. Positional refinement was begun using data to 3.5-Å resolution and then increased in stages to the limit of resolution, using the program TNT (48). Electron density maps ($2F_o - F_c$ and $F_o - F_c$) were analyzed using the program O (49). B-factor refinement was performed using the default TNT B-factor correlation library. Solvent molecules were added only if indicated by large positive features in the ($F_o - F_c$) electron density maps and in reasonable proximity of hydrogen bond partners.

The free R-factor was determined *a posteriori* (50) from 10% of the diffraction data after simulated annealing refinement against the remaining 90% of the data. To verify structural details in the vicinity of the introduced disulfides, "omit" ($F_o - F_c$) difference electron density maps were calculated after removing small segments from the model and subjecting the remaining portions to simulated annealing refinement prior to phase calculation.

Mitochondrial Expression of roGFP1 and Spectroscopy of Cell Suspensions—A stable line of HeLa cells expressing roGFP1 in the mitochondrial matrix was created by transfection with the pEGFP-N1/roGFP1 plasmid containing the pyruvate dehydrogenase E1α subunit leader sequence and by selection of colonies exhibiting green fluorescence in the presence of G418 (Calbiochem). Cells were grown to 100% confluence on a 15-cm tissue culture plate (HG-DMEM medium plus 10% fetal calf serum; Invitrogen), treated with trypsin briefly to release, and then were washed, harvested, and suspended in 4.0 ml of phosphate-buffered saline buffer (10 mM sodium/potassium phosphate, pH 7.4, 137 mM NaCl, 2.7 mM KCl, 0.5 mM $CaCl_2$, 0.5 mM $MgCl_2$, and 25 mM glucose). 2 ml of cell suspension was transferred to a cuvette, and fluorescence excitation spectra were collected using a Hitachi F4500 fluorescence spectrophotometer with gentle stirring. To determine whether useful signals could be obtained with exogenous oxidants and reductants, either H_2O_2 (to 1 mM) or DTT (to 10 mM) were added. These reagents were chosen because of their apparent ability to fully oxidize and reduce samples of the purified roGFP1 protein *in vitro*. Fluorescence excitation scans were collected from 350 to 500 nm (2.5-nm slit widths, 510-nm emission) before and each minute after the addition of either 1 mM H_2O_2 or 10 mM DTT. As a control, cells not expressing roGFP1 were grown under identical conditions and subjected to the same procedure. Background subtraction was performed after correcting the emission spectra for the difference in cell density, as determined by measurements of A_{595} in the stirred cuvette.

[2] C. T. Dooley, T. M. Dore, G. Hanson, W. C. Jackson, S. J. Remington, and R. Y. Tsien, submitted for publication.

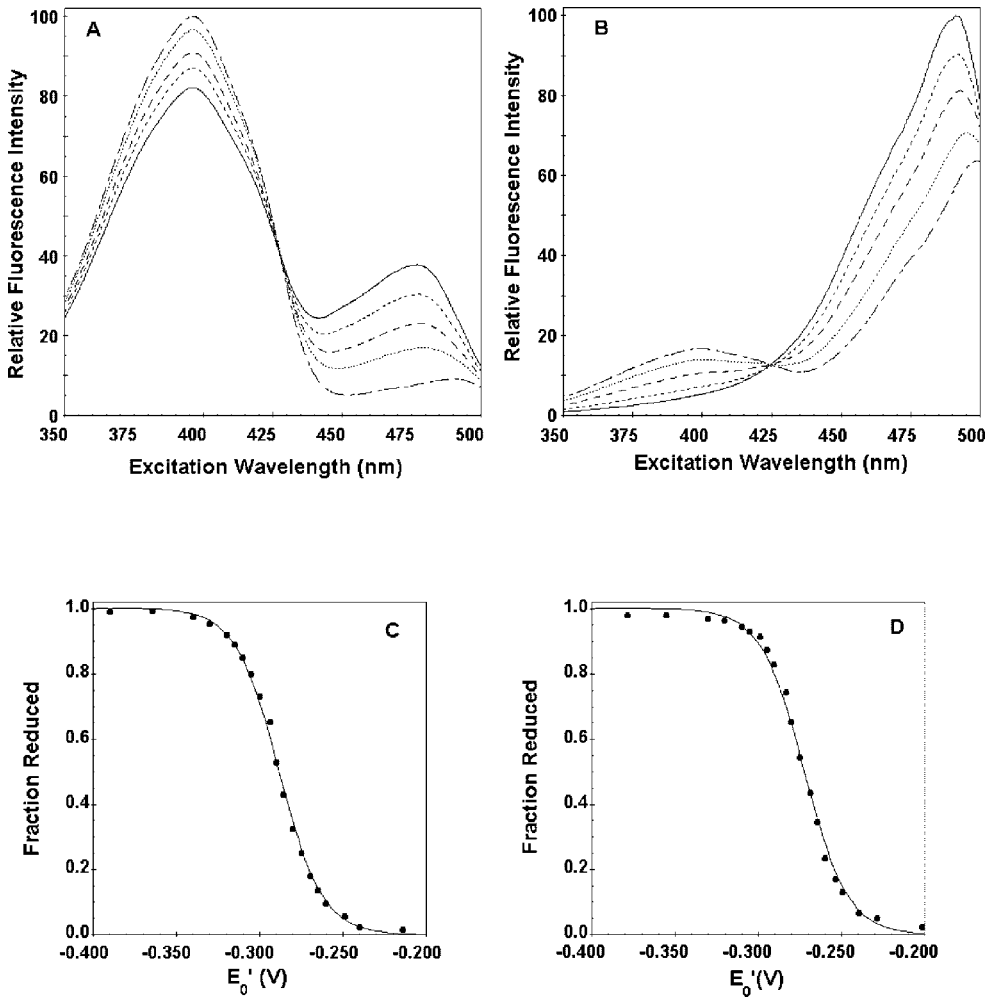

FIG. 1. **Redox equilibria of roGFPs by titration against DTT.** *A*, fluorescence excitation spectra of roGFP1 while monitoring emission intensity at 508 nm at the following redox potential values: −0.320 (*solid line*), −0.294 (*short dashed line*), −0.286 (*long dashed line*), −0.275 (*dotted line*), and −0.249 V (*dotted* and *dashed line*). *B*, fluorescence excitation spectra of roGFP2 while monitoring emission intensity at 511 nm at the following redox potential values: −0.310 (*solid line*), −0.285 (*short dashed line*), −0.275 (*long dashed line*), −0.265 (*dotted line*), and −0.240 V (*dotted and dashed line*). Fluorescence emission intensities were normalized to the maximum intensity recorded in each series of scans. *C* and *D*, apparent redox potential values of the roGFPs were determined by plotting the fraction of reduced protein *versus* the ratio of DTT_{red} to DTT_{ox} or the equivalent redox potential values and fitting the data to a titration curve.

Investigation of Mitochondrial Redox Status in Single Mammalian Cells Using Fluorescence Microscopy—HeLa cells stably transfected with pEGFP-N1/roGFP1 plasmid containing the pyruvate dehydrogenase E1α subunit leader sequence using Fugene (Roche Applied Science) were viewed with a × 60 dipping objective and imaged on a motorized Zeiss Axioscope 2 microscope. The temperature of the cells was maintained at 37 °C using an open perfusion microincubator (Harvard Apparatus Inc., Holliston, MA). Dual excitation ratio imaging required 400 (10) nm (Edmund Industrial Optics, Barrington, NJ) and D480/× 30 excitation filters, a 505DCXR dichroic mirror, and a D535/40 nm emission filter (Omega Optical and Chroma Technologies, Brattleboro, VT) alternated by a fast filter changer. Images were collected with a PentaMax cooled CCD camera (Princeton Instruments). Data were collected and processed using the program Openlab (Improvision, Lexington, MA). Fluorescence excitation ratios were obtained by dividing integrated intensities obtained from manually selected portions of the imaged regions of intact whole cells collected using 400 (10) nm and 480 (30) nm excitation filters after appropriate background correction. Background correction was performed by subtracting the intensity of a nearby cell-free region from the signal of the imaged cell.

RESULTS

Characterization of roGFPs—Fluorescence scans of roGFPs at different redox potentials were initially collected in 1 mM DTT redox buffer prepared by varying the ratio of reduced (DTT_{red}) to oxidized DTT (DTT_{ox}). Neither wild-type GFP nor any of the single Cys point mutants showed a significant change in fluorescence in response to the addition of oxidizing or reducing agents (data not shown), However, each of the double cysteine mutants responded strongly and rapidly to the oxidation state of the solution.

For each, two excitation maxima (at about 400 and 475–490 nm) as in wild-type GFP were observed. These maxima are attributed to an internal equilibrium between the neutral and anionic forms of the chromophore, respectively (22). However, unlike wild-type GFP, in roGFPs the relative amplitudes of these peaks depend strongly on the solution oxidation potential. The fluorescence excitation spectra of roGFP1 and -2 are shown in Fig. 1, *A* and *B*. The spectra show that formation of the disulfide favors the protonated, neutral form of the chromophore. For roGFP1, oxidation increases the 400-nm excitation peak (band A) while decreasing the 475-nm peak (band B). A clean isosbestic point separating the two peaks is observed at 425 nm, indicative of two equilibrating molecular species. The fluorescence excitation spectrum of roGFP2 (roGFP1 with the addition of the S65T mutation) (Fig. 1*B*) responds in a similar manner, but the relative amplitudes of the A (400-nm) and B (490-nm) bands are reversed.

In contrast to roGFP1, roGFP2 fluorescence emission depends on pH as well as redox potential. This is not surprising, since most GFP variants containing the S65T mutation are

TABLE I
Spectroscopic excitation ratios and redox equilibrium properties of roGFPs

Variant[a]	ID	K_{eq}[b]	E'_0[c]	δ[d]
			V	
S147C/Q204C	roGFP1	0.070	−0.288	6.1[e]
S147C/Q204C[f]	roGFP1	0.83[f]	−0.287	4.5[e]
S147C/Q204C/S65T	roGFP2	0.021	−0.272	5.8[g]
N149C/S202C	roGFP3	0.151	−0.299	4.3[e]
N149C/S202C/S65T	roGFP4	0.056	−0.286	2.6[g]
S147C/Q204C/N149C/S202C	roGFP5	0.134	−0.296	7.8[e]
S147C/Q204C/N149C/S202C/S65T	roGFP6	0.039	−0.280	5.4[g]

[a] Variants in this column also contain the two phenotypically neutral substitutions C48S and Q80R.
[b] Equilibrium constant (K_{eq}) values are given for the reaction $roGFP_{red} + DTT_{ox} \leftrightarrows roGFP_{ox} + DTT_{red}$ (see exception below for lipoic acid in Footnote *f*).
[c] E'_0 values are for pH 7 and 30 °C.
[d] The dynamic range value (δ) is the maximum observed δ-fold change in excitation peak ratio.
[e] Measured at 475 and 400 nm.
[f] Values estimated by titration against lipoic acid (assumed midpoint potential, −290 mV), average of two experiments.
[g] Measured at 490 and 400 nm.

sensitive to pH variations and at low pH are only weakly or not at all fluorescent (51). The pK_a of roGFP2 depends somewhat on the oxidation state (data not shown), and the values were determined by titration to be about 5.6 (reduced) and 6.0 (oxidized).

The redox midpoint potentials of the various roGFPs were determined from the equilibrium constant obtained by fitting a theoretical curve to a plot of the fraction of reduced protein *versus* the ratio of DTT_{red} to DTT_{ox} (*e.g.* Fig. 1, *C* and *D*). This gave values of −0.288 and −0.272 V for roGFP1 and -2, respectively. Table I summarizes various spectroscopic and biochemical properties of six roGFPs. As a check, titration of roGFP1 against the lipoic acid/dihydrolipoic acid (E'_0 = −290 mV) couple was performed in two completely independent experiments using a procedure described elsewhere[2] and resulted in very similar values (−0.285 and −0.288 V) for the midpoint potential. As can be seen from Table I, K_{eq}, E'_0, and δ, the dynamic range parameter, depend upon the specific sites of substitution as well as upon the background used (*i.e.* S65T).

The pH dependence of the midpoint potential for roGFP2 was investigated for several points in the pH range 6.0–8.0 at 30 °C and found to correspond linearly to pH according to the expression $E'_0{}^{pH} = E'_0 - 65.5\ mV \times (pH - 7.0)$ (correlation coefficient $R = 0.9999$; data not shown). Thus, the pH dependence does not correspond precisely to the simple model expressed by Equation 7, possibly because of the presence of nearby titratable groups in the protein (52).

Crystal Structure Analyses of roGFP2—roGFP2 (S147C/Q204C/S65T/F64L) crystallized readily and was therefore used for the structure analysis. Crystals of both reduced and oxidized forms were investigated in order to better understand how disulfide bond formation leads to changes in the fluorescence excitation spectrum. The crystals belong to the space group $P2_12_12$, and the structures were solved by molecular replacement to 1.9-Å resolution for the oxidized form and 2.0-Å resolution for the reduced form. roGFP2 crystallized as a dimer, with three molecules in the asymmetric unit of the crystal. Each individual monomer is essentially identical to the S65T structure used as a search model (Protein Data Bank code 1EMA). One molecule (the A monomer; Fig. 2*A*) is related to its dimer partner by a crystallographic 2-fold axis of symmetry, whereas the other two molecules in the asymmetric unit (B and C) are related by a noncrystallographic 2-fold axis of symmetry. The dimer interface is essentially the same as seen for wild-type GFP (53) and YFP (54). Since the resolution limit of the data collected was reasonably high, refinement was performed without imposing noncrystallographic symmetry restraints. Thus, the three molecules in the asymmetric unit provide three independent views of the protein in different crystal packing environments. Backbone atoms from any pair of monomers superimpose to an accuracy of about 0.33 Å root mean square.

Final model statistics are presented in Table II. The geometry is acceptable, but the crystallographic *R*-factors (Table II) are somewhat higher than satisfactory because of an unusual type of disorder in the crystals. Although the electron density for the A and B molecules was very clear, the electron density was poorly defined for a fairly extensive surface region of the C molecule. Consequently, portions of this region (C-subunit residues in the ranges 24–31, 47–54, 72–74, 110–123, 133–138, 155–160, 188–198, and 209–217) were difficult to model, and many side chains had to be truncated. This region faces a large solvent cavity, which is probably responsible for the apparent disorder. It seems likely that the disorder arises from dynamic rotation or static disorder of the C molecule about the 2-fold axis along the B-C interface. Atomic coordinates and structure factors have been deposited in the Protein Data Bank (available on the World Wide Web at www.rcsb.org/) and may be retrieved using access codes 1JC0 and 1JC1.

The introduced cysteines face the bulk solvent (Fig. 2*A*) and form a disulfide with full occupancy under oxidizing conditions. In the crystal, they are near one edge of the dimer interface, but the two pairs of cysteines in the dimer are separated by at least 14 Å (the closest adjacent molecule) and so cannot form intermolecular disulfides during crystallization. In the oxidized crystals, the electron density distribution reveals that the disulfide bond is completely formed and well ordered (Fig. 2*B*). In the reduced crystals, careful analysis revealed that despite the care used in handling the crystals, partial oxidation of Cys^{147} and Cys^{204} took place, presumably during data collection as a result of x-ray irradiation. Given that the resolution was not high enough to resolve the individual components, the final structure was successfully modeled as a superposition of two partially occupied states each enforced by appropriate stereochemical restraints (see *bottom panel* of Fig. 2*B*). The occupancy factors were adjusted manually during several rounds of refinement and inspection of ($F_o - F_c$) omit difference electron density maps, with *B* values fixed at the average for the entire residue. From this procedure, we estimated that 25–35% of the molecules in the reduced crystal formed disulfides, for each of the A, B, and C molecules. In the final model, this fraction was fixed at 30% oxidized and 70% reduced for each of the three molecules.

It is clear that when reduced, the Sγ of Cys^{204} moves away from the Sγ of Cys^{147}, which occupies approximately the same position in either oxidation state (Fig. 2*B*, *top* and *bottom*). At neither cysteine is there evidence of alternative conformations, further oxidation by molecular oxygen, or cross-links with other compounds in either crystal.

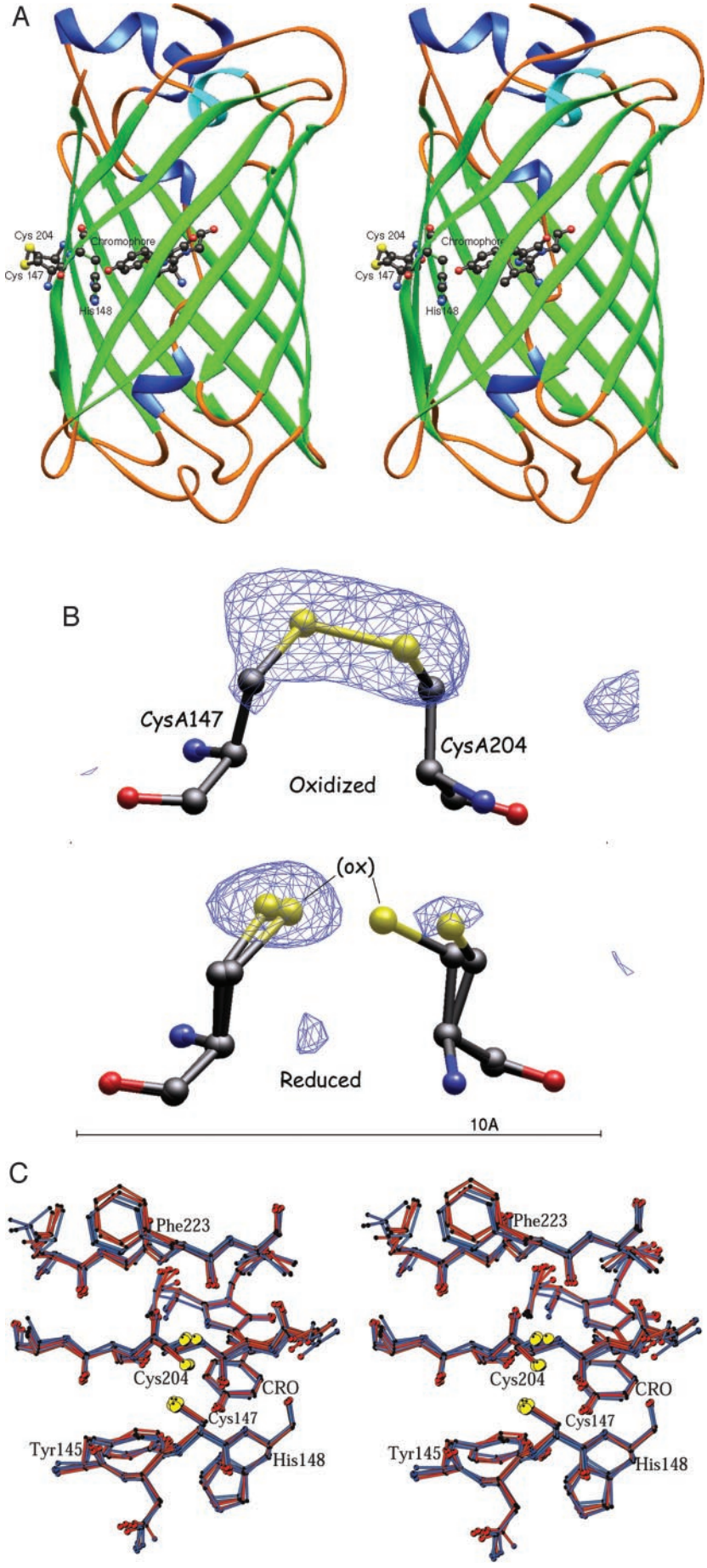

FIG. 2. **Key structural features of roGFP2, figures produced by RIBBONS (63) and MOLSCRIPT (1).** *A*, the engineered cysteines Q204C/S147C form a disulfide cross-link between adjacent β-strands near the chromophore in GFP. The atomic model of the two cysteine residues, His^{148} and the chromophore are in the *ball-and-stick* representation (nitrogen atoms *blue*, oxygen *red*, sulfur *yellow*, and carbon *gray*). *B*, *top panel*, portion of the ($F_o - F_c$) simulated annealing omit electron density map of the oxidized crystals, after removal of Cβ and Sγ from residues 147 and 204. Contour level = +3 σ (there are no negative features at this contour level). The final refined atomic model is superimposed as a *ball-and-stick* model. *Bottom panel*, portion of the ($F_o - F_c$) simulated annealing omit electron density map of the reduced crystals, after removal of atoms Cβ and Sγ from residues 147 and 204 of the reduced partial model. In this map, the partial model of the oxidized disulfide linkage was included for phasing at 30% occupancy. Peaks show locations of the Sγ atoms of the reduced partial model, contour level +3 σ. No negative electron density features are present at this contour level. *C*, *ball-and-stick* stereo view of a superposition of the six molecules (three oxidized, three reduced) in the asymmetric unit of the crystals (*red bonds*, oxidized; *blue bonds*, reduced). Shown are oxidation state-dependent rearrangements of segments of the protein in the immediate vicinity of the disulfide bridge and the fluorophore (*CRO*). The features of interest are a slight contraction of the main chain upon disulfide bridge formation and concomitant rearrangements of the side chains of Phe^{223} and the Sγ of Cys^{204}.

TABLE II
Data collection and refinement statistics for oxidized and reduced roGFP2

Data collection	Oxidized	Reduced
Crystal		
Total observations	203,865	194,884
Unique reflections	56,854	38,346
Cell dimensions (*a*, *b*, *c*) (Å)	186.8, 67.6, 56.1	185.6, 67.9, 56.4
Resolution (Å)	29.7–1.90	28.7–2.00
Highest resolution shell (Å)	1.95–1.90	2.10–2.00
Completeness[a] (%)	99.8 (100)	78.2 (74.3)
Multiplicity[a]	3.6 (3.6)	5.1 (5.5)
Average $I/\sigma(I)$[a]	7.2 (2.3)	8.7 (2.2)
R_{merge}[a,b]	0.058 (0.247)	0.053 (0.304)
Refinement		
Space group	$P2_12_12$	$P2_12_12$
No. of molecules[c]	3	3
No. of protein atoms[c]	5,194	5,216
No. of solvent atoms[c]	216	132
Resolution range (Å)[d]	6.0–1.9	6.0–2.0
Crystallographic *R*-factor[e] (reflections)	0.226 (54,921)	0.224 (36,454)
R-free (reflections)	0.317 (5471)	0.329 (3593)
Average *B*-factors (Å^2)		
Protein atoms	42.5	43.5
Solvent	42.2	40.4
Root mean square deviations from ideality		
Bond lengths (Å)	0.012	0.011
Bond angles (degrees)	2.1	2.0
B-factor correlations (Å^2)	4.7	5.2

[a] Values in parentheses indicate statistics for the highest resolution shell.
[b] $R_{merge} = \Sigma I\langle I\rangle / \Sigma\langle I\rangle$, where I is the observed intensity, and $\langle I\rangle$ is the average of intensities obtained from multiple observations of symmetry-related reflections.
[c] Per asymmetric unit.
[d] Due to an inadequate solvent model, reflections from 30 to 6 Å were excluded. All other reflections in the resolution range were used; no σ or intensity cut-off was applied.
[e] R-factor $= \Sigma||F_o|-|F_c||/\Sigma|F_o|$, where F_o and F_c are the observed and calculated structure amplitudes, respectively.

The disulfide bond present in the oxidized roGFP2 structure (Fig. 2) has the pg^-g^- conformation typical of linkages between two antiparallel β-strands (55) but has highly strained geometry. Averaged over the three molecules in the asymmetric unit, the descriptive parameters are as follows: average C_α–C_α distance of 4.04 ± 0.09 Å, C_β–C_β distance of 4.19 ± 0.03 Å, S–S distance of 1.97 ± 0.06 Å, C_α–C_β–S angle of 112 ± 1.4°, C_β–S–S angle of 105.6 ± 1.7°, and a C_β–S–S–C_β torsion angle of 115.7 ± 0.6°. Torsion angle restraints were not applied during crystallographic refinement. These parameters deviate significantly from those seen for naturally occurring disulfides, even for the naturally strained disulfides that are occasionally found between adjacent antiparallel β-strands. Srinivasan *et al.* (55) did not present S.D. values in their very useful statistical analysis of disulfide geometry in proteins. However, the average value of the SS torsion angle of ~116° in roGFP2 is clearly on the extreme edge of the observed distribution centered at about 90° (see Fig. 3*A* of Srinivasan *et al.* (55)). Likewise, the short Cα–Cα distance of 4.04 Å is on the lower edge of the observed bimodal distribution, which peaks at about 5.1 and 5.7 Å. Finally, the 4.19-Å C_β–C_β distance is unusually long compared with the more typical 3.8 Å. Presumably, the degree of strain in the disulfide linkage varies between different roGFPs, and this may account for the observed differences in midpoint potentials.

The strain of disulfide bridge formation appears to result in small but significant movements on the part of both the main chain and side chains in its vicinity. For comparison, six independent subsets of molecular segments each consisting of peptides 145–147, 202–206, 220–224, and the chromophore were superimposed using carbon atoms of reduced molecule A as the reference. The resulting root mean square deviations were 0.43–0.67 Å for 88 atoms, which reflects significant structural changes. The result is shown as a collection of *ball-and-stick models* (Fig. 2*C*) in which *red bonds* correspond to oxidized structures, and *blue bonds* correspond to reduced structures.

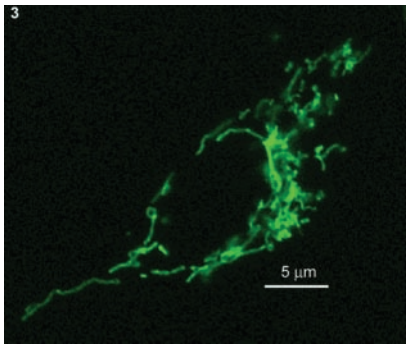

FIG. 3. **Single cell image of roGFP1 targeted to HeLa cell mitochondria obtained by fluorescence microscopy.** The image shows a single cell and reveals the mitochondrial localization pattern of roGFP1. Note the reticular nature of mitochondria.

With the caveat of partial oxidation of the "reduced" crystal, the Phe^{223} phenyl ring can be seen to shift in response to the movement of Cys^{204} Sγ upon reduction. This appears to result from a small relative movement of main chain residues 221–225 rather than from steric clash with the Cys^{204} side chain, since the closest side chain distances are >5 Å. The Cys^{147}–Cys^{204} Cα–Cα distance shrinks from 4.30 ± 0.12 to 4.04 ± 0.09 Å (difference >2 σ or $p > 0.95$) upon oxidation. These differences, although not large, are significant and suggest that disulfide bridge formation introduces a degree of structural strain into the molecule and hence into the chromophore environment. Finally, it should be pointed out the His^{148} and Ser^{205}, which contact the chromophore, are immediately adjacent to the introduced cysteine residues 147 and 204 and would be expected to shift positions as a result of disulfide bond formation. As a result, it is reasonable to suppose that changes in the chromophore environment perturb the equilibrium between the neutral and anionic forms of the chromophore.

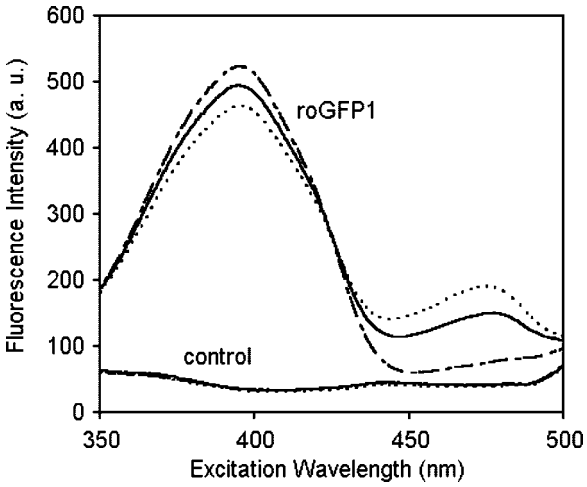

FIG. 4. **Fluorescence excitation spectra of HeLa cell suspensions with emission response on an arbitrary scale.** HeLa cells were stably transfected with roGFP1. The initial spectrum (*solid line*), the spectrum after 1 mM H_2O_2 addition (*dashed line*), and the spectrum after 10 mM DTT addition (*dotted line*) are shown. The curves labeled *control* show fluorescence excitation spectra of untransfected HeLa cells and indicate the relative intensity of autofluorescence. Spectra were collected while monitoring emission at 510 nm and corrected for relative cell density in the suspension.

Investigation of Mitochondrial Redox Potential in Cell Suspensions—The ability of the roGFPs to monitor redox state in cells was examined using HeLa cells stably transfected with roGFP1. The leader sequence of the E1α subunit of pyruvate dehydrogenase was used to direct the protein into the matrix of mitochondria. Fluorescence microscopy verified expression exclusively in mitochondria (Fig. 3). The ability of the roGFPs to report redox state in intact cells in suspension was examined using a Hitachi F4500 fluorescence spectrophotometer. As shown in Fig. 4, the fluorescence excitation spectra of roGFP1 are readily detectable in cell suspension and altered by the addition of a strong reductant DTT or oxidant H_2O_2. Cellular autofluorescence, presumed to be due to the presence of NAD(H) and FAD, while measurable, is small compared with the probe fluorescence. Finally, unmodified cells do not show observable change in fluorescence upon the addition of H_2O_2 or DTT (*dashed* and *dotted lines* in control). From analysis of the data presented in Fig. 4 (including background subtraction from the control measurement), the roGFP1 probe is on average 89% reduced in HeLa cell mitochondria under the conditions of cell suspension.

Investigation of Mitochondrial Redox Status in Single Living Cells—Studies using cell suspensions estimate the average redox state in a cell population. However, cells in culture are rarely synchronized for cell cycle stage or metabolic responses, so it is important that redox properties be measurable in single living cells. Analysis of the response of roGFP1 in single living cells was performed using a Zeiss Axioscope 2 microscope as described under "Materials and Methods." Imaged regions were manually chosen and included primarily those regions apparently comprising the mitochondria. The addition of 1 mM H_2O_2 and 10 mM DTT (Fig. 5) evoked qualitatively similar responses to the experiments conducted in the fluorometer using cell suspensions. The initial 400/480 nm ratio, obtained from measurements on 23 cells in seven independent microscopy experiments, was found to correspond to 67 ± 7% reduction of roGFP1. Assuming that roGFP1 is fully reduced or oxidized in the cell by the added reductants or oxidants and that roGFP1 responds quantitatively the same *in vivo* as it does *in vitro*, the estimated E_0' of the mitochondrial matrix is −0.298 ± 0.004 V at the standard conditions of pH 7 and 30 °C.

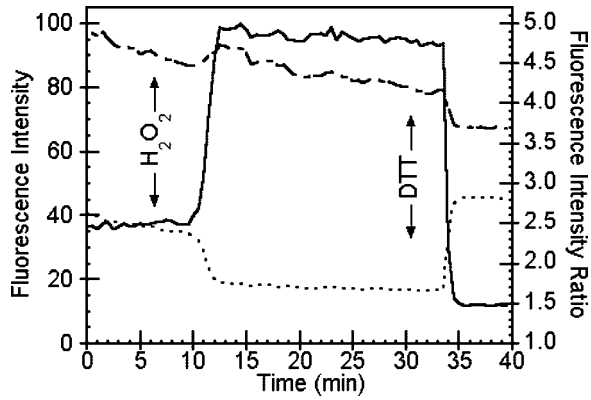

FIG. 5. **Fluorescence intensity response of roGFP1 to exogenous H_2O_2 and DTT, within the mitochondrion of a single living HeLa cell as obtained by image processing.** The individual 400-nm (*short and long dashed line*) and 480-nm (*short dashed line*) excitation channels were normalized to the maximum value of the 400-nm channel. The 400/480-nm ratio (*solid line*) is also shown. The *arrows* indicate the times at which DTT and H_2O_2 were added.

The pH of mitochondria has been estimated to be 7.98 (26), so from Equation 7, the corrected redox potential at pH 7.98 and 37 °C is estimated to be approximately −360 mV. This correction for the pH dependence is based on the assumption that the introduced cysteine residues have individual pK_a values significantly greater than 8.0, which is the case. In work to be published elsewhere,[3] the apparent pK_a values for the forward and reverse rates of disulfide formation have been determined for several roGFPs. These values were found to be greater than 9.0 and thus significantly higher than the textbook value of 8.33 for the cysteine side chain in solution, although protein instability at high pH precluded a more accurate determination.

DISCUSSION

Redox-sensitive GFP indicators were successfully created by introduction of disulfides close to a conspicuous bulge in the otherwise regular GFP β-barrel. The bulge is centered on His^{148}, the side chain of which partially fills the bulge and interacts with the chromophore phenol(ate) oxygen (34, 51, 56) (see Fig. 2*A*). Modifications to the location, including insertion of entire peptides (29, 57), are known to dramatically alter the spectroscopic properties of GFP and yet yield functional fluorescent proteins. Crystal structure analyses verified reversible formation of the disulfide for roGFP2 and also suggested that localized geometric strain caused by disulfide formation propagates toward the chromophore region, which presumably accounts for the redox-dependent shifts in the excitation spectrum. Consequently, the design principle is validated. The atomic model for roGFP2 is expected to be an excellent approximation to that of the mitochondrially expressed roGFP1 because each contains the critical 147/204 disulfide linkage.

Ostergaard *et al.* (33) investigated four sites for introduction of disulfides in a YFP background, including the two discussed here (149–202 and 147–204) and reported similar success. However, in YFP, the protonated form of the chromophore does not fluoresce, and consequently, the oxidation state affects only the intensity of fluorescence. The probes thus do not permit ratiometric measurements. The 149–202 pair was investigated in detail, and the midpoint potential was reported to be −261 mV by titration against the GSH/GSSG couple. This value is less negative than those reported here for the variants roGFP3 (−299 mV) or roGFP4 (−286 mV), which contain the same disulfide. Although the constructions are not strictly compara-

[3] M. Cannon and S. J. Remington, manuscript in preparation.

ble due to the different backgrounds, the disulfide in $rxYFP^{149}{}_{202}$ is still a very reducing and stable disulfide linkage, in agreement with our results.

In comparing the results reported here and elsewhere,[2] we find the midpoint potentials determined for roGFPs to be in reasonable agreement. However, Dooley *et al.*[2] consistently report somewhat more negative values for the midpoint potentials. We have compared data sets but are not yet able to account for these small discrepancies, which may be due to variations in sample preparation or reagents. It should be noted that the results reported here were not corrected for possible partial air oxidation that may have been present in the fully reduced DTT and/or lipoate samples and thus may result in less reducing (*i.e.* more positive values) of the midpoint potentials. For practical purposes, we suggest using consensus values of −291 and −280 mV for the midpoint potentials of roGFP1 and roGFP2, respectively.

The unusually negative midpoint potentials of roGFP probes will be disadvantageous for use in oxidizing compartments such as the endoplasmic reticulum; however, the observed midpoint potentials depend on the sites of disulfide substitution. Although the midpoint potentials of the redox-active cysteines in the active sites of thioredoxins and reductases have been subjected to some scrutiny (52, 58), the factors that control the equilibrium constants for protein disulfide formation are not well understood. Zhang and Snyder (59) studied disulfide formation in small peptides and observed that both geometric and entropic effects control the equilibrium constant for loop closure. Given the crystallographic determination of geometric strain in the 147–204 linkage as discussed previously, we are not able to offer a quantitative explanation for the unusual stability of the 147–204 or 149–202 linkages. Presumably there are other locations in GFP suitable for the introduction of disulfides that would permit less reducing linkages to form, as suggested by the work of Ostergaard *et al.* (33). Such constructions could in principle provide fluorescent redox probes suitable for use in more oxidizing environments.

One of the more important roGFP features is the ratiometric variation of fluorescence excitation, which is caused by an increase in the chromophore protonation state upon oxidation. This behavior has the potential of reducing or eliminating distortions of data caused by photobleaching, indicator concentration, illumination stability, excitation path length, and nonuniform indicator distribution within cells or between groups of cells (35, 60). It should be emphasized that these ratios are sensitive to the wavelengths chosen and to the characteristics of the individual instrument, such as source intensity profiles, excitation bandwidth, and detector sensitivity. For this reason, individual calibration curves should be obtained for each probe under the conditions used for the experimental measurements. The "pseudo-wild-type" roGFPs (roGFP1, -3, and -5) with more closely matched excitation peak amplitudes may aid in fluorescence microscopy experiments by allowing the same camera/detector settings to capture both images that constitute the ratio. These probes offer the additional advantage that the probe response is relatively insensitive to variations in pH.

In cell expression experiments, roGFP1 is clearly in equilibrium with the redox potential of mitochondrial matrix, which is readily altered by the addition of membrane-permeable redox agents. In the present study, we were able to demonstrate that roGFP1 is initially neither fully oxidized nor fully reduced in the mitochondrial matrix of HeLa cells as shown by the response to the addition of H_2O_2 and DTT. In these cells and under these growth conditions, the redox potential of the resting mitochondria lies within the effective range of the probe. Therefore, studies of redox changes in response to altered metabolic conditions or exogenous reagents can be performed in cell suspensions using the probes described here. The estimated value of −360 mV for the mitochondrial redox potential corresponds to very reducing conditions, but it should be considered that cells in culture and cancer cells, such as HeLa cells in particular, are living primarily by glycolysis with little or no contribution from oxidative phosphorylation. Under such circumstances, the ratio of NADH to NAD^+ and, therefore, the levels of reducing equivalents will be high.

Indeed, in similar experiments, we showed elsewhere (61, 62) that the redox state of mitochondrially expressed roGFP1 depends on the cell growth medium. roGFP1 was substantially more reduced (92%) in HeLa cells grown in glucose medium than in the same cells grown in galactose/glutamine medium (82%). This result is expected, because the simultaneous presence of galactose and glutamine forces the cells to utilize the Krebs cycle and consequently decreases the $NADH/NAD^+$ ratio. Such results are very promising for the use of these probes as monitors of metabolism-dependent redox changes *in vivo*.

Finally, the probes respond to the presence of reactive oxygen species such as H_2O_2, which is an important issue for researchers studying aging, signal transduction, and neurodegenerative diseases.

In Vitro Applications—Redox-sensitive GFPs will be excellent tools for a variety of *in vitro* applications. Since chromophore fluorescence is dependent upon the extent of disulfide bond formation as well as the energy of formation (E'_0 value) of the disulfide bond, roGFPs provide a useful model system to study disulfide bond stability and rates of formation. Such studies might involve exchange reactions with different model compounds or redox-active proteins. In principle, disulfide exchange rates and oxidation or reduction rates of redox-active compounds could be determined by fast fluorometric (stopped-flow) techniques. roGFPs could also be used as a fluorescent standard for measurement of the apparent redox midpoint potential and exchange rates of other redox-active compounds of biological relevance.

Acknowledgments—We thank K. Kallio for help with crystallization of roGFP2/F64L and K. Chicas-Cruz for expertise in cell culture work.

REFERENCES

1. Kraulis, P. J. (1991) *J. Appl. Crystallogr.* **24,** 946–950
2. Frand, A. R., and Kaiser, C. A. (1998) *Mol. Cell* **1,** 161–170
3. Pollard, M. G., Travers, K. J., and Weissman, J. S. (1998) *Mol. Cell* **1,** 171–182
4. Sevier, C. S., Cuozzo, J. W., Vala, A., Aslund, F., and Kaiser, C. A. (2001) *Nat. Cell Biol.* **3,** 874–882
5. Gross, E., Sevier, C. S., Vata, A., Kaiser, C. A., and Fass, D. (2002) *Nat. Struct. Biol.* **9,** 61–67
6. Frand, A. R., and Kaiser, C. A. (1999) *Mol. Cell* **4,** 469–477
7. Tu, B. P., and Weissman, J. S. (2002) *Mol. Cell* **10,** 983–994
8. Frand, A. R., Cuozzo, J. W., and Kaiser, C. A. (1998) *Trends Cell Biol.* **10,** 203–210
9. Debarbieux, L., and Beckwith, J. (1999) *Cell* **99,** 117–119
10. Cuozzo, J. W., and Kaiser, C. A. (1999) *Nat. Cell Biol.* **1,** 130–135
11. Dickinson, D. A., and Forman, H. J. (2002) *Ann. N. Y. Acad. Sci.* **973,** 488–504
12. Ritz, D., and Beckwith, J. (2001) *Annu. Rev. Microbiol.* **2001,** 21–48
13. Shi, Y. (2001) *Nat. Struct. Biol.* **8,** 394–401
14. Chernyak, B. V. (1997) *Biosci. Rep.* **17,** 293–302
15. Hall, A. G. (1999) *Eur. J. Clin. Invest.* **29,** 238–245
16. Cai, J., and Jones, D. P. (1999) *J. Bioenerg. Biomemb.* **31,** 327–334
17. Rhee, S. G., Bae, Y. S., Lee, S. R., and Kwon, J. (2000) *Science's STKE* http://stke.sciencemag.org/cgi/content/full/sigtrans;2000/53/pe1
18. Claiborne, A., Yeh, J. I., Mallet, T. C., Luba, J., Crane, J. E., Charrier, B., and Paronage, D. (1999) *Biochemistry* **38,** 15407–15416
19. Demple, B. (2002) *Mol. Cell Biochem.* **234,** 11–18
20. Hwang, C., Sinskey, A. J., and Lodish, H. F. (1992) *Science* **257,** 1496–1502
21. Keese, M. A., Saffrich, R., Dandekar, T., Becker, K., and Schirmer, R. H. (1999) *FEBS Lett.* **447,** 135–138
22. Tsien, R. Y. (1998) *Annu. Rev. Biochem.* **67,** 509–544
23. Remington, S. J. (2000) *Methods Enzymol.* **305,** 195–211
24. Zimmer, M. (2002) *Chem. Rev.* **102,** 759–781
25. Kneen, M., Farinas, J. F., and Verkman, A. S. (1998) *Biophys. J.* **74,** 1591–1599
26. Llopis, J., McCaffery, J. M., Miyawaki, A., Farquhar, M., and Tsien, R. Y. (1998) *Proc. Natl. Acad. Sci. U. S. A.* **95,** 6803–6808
27. Nagai, T., Sawano, A., Park, E. S., and Miyawaki, A. (2001) *Proc. Natl. Acad. Sci. U. S. A.* **98,** 3197–3202

28. Miesenbock, G., De Angelis, D. A., and Rothman, J. E. (1998) *Nature* **394,** 192–195
29. Baird, G. S., Zacharias, D. A., and Tsien, R. Y. (1999) *Proc. Natl. Acad. Sci. U. S. A.* **96,** 11241–11246
30. Miyawaki, A., Griesbeck, O., Heim, R., and Tsien, R. Y. (1999) *Proc. Natl. Acad. Sci. U. S. A.* **96,** 2135–2140
31. Jayaraman, S., Haggie, P., Wachter, R. M., Remington, S. J., and Verkman, A. S. (2000) *J. Biol. Chem.* **275,** 6047–6050
32. Hanson, G. T., McAnaney, T. B., Park, E. S., Rendell, M., Yarbrough, D. K., Chu, S., Xi, L., Boxer, S. G., Montrose, M. H., and Remington, S. J. (2002) *Biochemistry* **41,** 15477–15488
33. Ostergaard, H., Henriksen, A., Hansen, F. G., and Winther, J. R. (2001) *EMBO J.* **20,** 5853–5862
34. Ormo, M., Cubitt, A. B., Kallio, K., Gross, L. A., Tsien, R. Y., and Remington, S. J. (1996) *Science* **273,** 1392–1395
35. Grynkiewicz, G., Martin, P., and Tsien, R. Y. (1985) *J. Biol. Chem.* **260,** 3440–3450
36. Wachter, R. M., and Remington, S. J. (1999) *Curr. Biol.* **9,** R628–R629
37. Wachter, R. M., Yarbrough, D., Kallio, K., and Remington, S. J. (2000) *J. Mol. Biol.* **301,** 157–171
38. Prasher, D. C., Eckenrode, V. K., Ward, W. W., Prendergast, F. G., and Cormier, M. J. (1992) *Gene* (*Amst.*) **11,** 229–233
39. Sowdhamini, R., Srinivasan, N., B., S., Santi, D. V., Ramakrishnan, C., and Balaram, P. (1989) *Protein Eng.* **3,** 95–103
40. Matsumura, M., Becktel, W. J., Levitt, M., and Matthews, B. W. (1989) *Proc. Natl. Acad. Sci. U. S. A.* **86,** 6562–6566
41. Cormack, B. P., Valdivia, R. H., and Falkow, S. (1996) *Gene* (*Amst.*) **173,** 33–38
42. Hawkins, H. C., De Nardi, M., and Freedman, R. B. (1991) *Biochem. J.* **275,** 341–348
43. Sajewski, R. P., and Whitesides, G. M. (1980) *J. Am. Chem. Soc.* **102,** 2011–2015
44. Lees, W. J., and Whitesides, G. M. (1991) *J. Org. Chem.* **58,** 642–647
45. Tsien, R. Y., and Poenie, M. (1986) *Trends Biochem. Sci.* **11,** 450–455
46. Leslie, A. G. W. (1996) in *Crystallographic Computing* (Moras, D., Podjarny, A. D., and Thierry, J. C., eds) Vol. 5, pp. 50–61, Oxford University Press, Oxford, UK
47. Kissinger, C. R., Gehlhaar, D. K., and Fogel, D. B. (1999) *Acta Crystallogr. Sec. D* **55,** 484–491
48. Tronrud, D. E., Ten Eyck, L. F., and Matthews, B. W. (1987) *Acta Crystallogr. Sec. A* **43,** 489–503
49. Jones, T. A., Zou, J.-Y., Cowan, S. W., and Kjeldgaard, M. (1991) *Acta Crystallogr. Sec. A* **47,** 110
50. Brunger, A. T. (1997) *Methods Enzymol.* **277,** 366–396
51. Elsliger, M.-A., Wachter, R. M., Hanson, G. T., Kallio, K., and Remington, S. J. (1999) *Biochemistry* **38,** 5296–5301
52. Wunderlich, M., and Glockshuber, R. (1993) *Protein Sci.* **2,** 717–726
53. Yang, F., Moss, L. G., and Phillips, G. N. J. (1996) *Nat. Biotechnol.* **14,** 1246–1251
54. Wachter, R. M., Elsliger, M. A., Kallio, K., Hanson, G. T., and Remington, S. J. (1998) *Structure* **6,** 1267–1277
55. Srinivasan, N., Sowdhamini, R., Ramakrishnan, C., and Balaram, P. (1990) *Int. J. Peptide Protein Res.* **36,** 147–155
56. Palm, G. J., Zdanov, A., Gaitanaris, G. A., Stauber, R., Pavlakis, G. N., and Wlodawer, A. (1997) *Nat. Struct. Biol.* **4,** 361–365
57. Topell, S., Hennecke, J., and Glockshuber, R. (1999) *FEBS Lett.* **457,** 283–289
58. Lin, T. Y., and Kim, P. S. (1989) *Biochemistry* **28,** 5282–5287
59. Zhang, R., and Snyder, G. H. (1989) *J. Biol. Chem.* **264,** 18472–18479
60. Whitaker, J. E., Haugland, R. P., and Prendergast, F. G. (1991) *Anal. Biochem.* **194,** 330–344
61. Capaldi, R. A., Aggeler, R., Gilkerson, R., Hanson, G., Knowles, M., Marcus, A., Margineantu, D., Marusich, M., Murray, J., Oglesbee, D., Remington, S. J., and Rossignol, R. (2002) *Biochim. Biophys. Acta* **155,** 192–195
62. Rossignol, R., Gilkerson, R., Aggeler, R., Yamagata, K., Remington, S. J., and Capaldi, R. A. (2004) *Cancer Res.* **64,** 985–993
63. Carson, M. (1987) *J. Mol. Graphics* **5,** 103–106